Front. Mech. Eng. 2022, 17(1): 7
https://doi.org/10.1007/s11465-021-0663-1

RESEARCH ARTICLE

Ultrasonic measurement of tie-bar stress for die-casting machine

Chaojie ZHUO[a,b], Peng ZHAO (✉)[a,b], Kaipeng JI[a,b], Jun XIE[a,b], Sheng YE[c], Peng CHENG[c], Jianzhong FU[a,b]

[a] *The State Key Laboratory of Fluid Power and Mechatronic Systems, College of Mechanical Engineering, Zhejiang University, Hangzhou 310027, China*
[b] *The Key Laboratory of 3D Printing Process and Equipment of Zhejiang Province, College of Mechanical Engineering, Zhejiang University, Hangzhou 310027, China*
[c] *Ningbo Haitian Die-Casting Equipment Co., Ltd., Ningbo 315821, China*

✉ *Corresponding author. E-mail: pengzhao@zju.edu.cn (Peng ZHAO)*

ABSTRACT In die casting, the real-time measurement of the stress of the tie-bar helps ensure product quality and protect the machine itself. However, the traditional magnetic-attached strain gauge is installed in the mold and product operating area, which hinders the loading and unloading of the mold and the collection of die castings. In this paper, a method for real-time measurement of stress using ultrasonic technology is proposed. The stress variation of the tie-bar is analyzed, and a mathematical model between ultrasonic signal and stress based on acoustoelastic theory is established. Verification experiments show that the proposed method agrees with the strain gauge, and the maximum of the difference square is only 1.5678 $(\mathrm{MPa})^2$. Furthermore, single-factor experiments are conducted. A higher ultrasonic frequency produces a better measurement accuracy, and the mean of difference squares at 2.5 and 5 MHz are 2.3234 and 0.6733 $(\mathrm{MPa})^2$, respectively. Measurement accuracy is insensitive to probe location and tonnage of the die-casting machine. Moreover, the ultrasonic measurement method can be used to monitor clamping health status and inspect the dynamic pulling force of the tie-bar. This approach has the advantages of high precision, high repeatability, easy installation, and noninterference, which helps guide the production in die casting.

KEYWORDS die-casting, tie-bar stress, acoustoelastic theory, ultrasonic measurement, dynamic inspection

1 Introduction

Recently, die casting has been widely used for manufacturing metallic components in many industries such as household appliances, automobiles, ships, and aerospace because of its advantages of high dimensional accuracy, high productivity, and near-net-shape [1–4]. In the automobile industry [5,6], lightweight alloy materials such as magnesium and aluminum are used widely to reduce body weight. Die casting is an important technology for processing lightweight alloys [7,8]. In die casting, the tie-bar must withstand reciprocating alternating stress. The magnitude of tie-bar stress may affect the quality of metallic components [9]. A small stress may produce defects such as flashes and poor geometrical accuracy, whereas a large stress could result in insufficient air venting during mold filling/packing, leading to generation of short shot. Traditionally, stress is set at the highest machine specification, which may lead to additional energy consumption [10]. Moreover, heavy loading at the tie-bars is detrimental to the durability of processed molds and the machine itself [11]. Therefore, the real-time measurement of stress in die casting is of great importance, which can be a reference for dynamic control of clamping force (The locking force of the mold formed by the template at the end of mold closing is numerically equal to the sum of the pulling force of the four tie-bars, and the unit is kN).

Stress optimization and load distribution on the four tie-bars are important indicators for evaluating the performance of the die-casting machine. A die-casting machine with evenly distributed load can ensure the quality of the product, protect the mold and the die-casting machine, and prolong the service life of the mold and the machine.

Received July 23, 2021; accepted October 24, 2021

Stress measurement is the precondition for the next step of regulation. The traditional measurement method measures the strain of the tie-bar with a sticky strain gauge and then calculates the stress of the tie-bar. However, the strain gauge is difficult to stick and can generally be used only once. The installation preparation time is up to 2–4 h [12]. The newly developed magnetic-attached strain gauge uses magnetic force instead of the adhesion of the traditional strain gauge, which solves the problems of disposability and long installation time. However, the strain gauge is installed in the mold and the product operating area, which hinders loading and unloading of the mold and the collection of die castings. Moreover, magnetic force decreases during die casting, which affects measurement accuracy. Therefore, it is not suitable for long-time measurement in the online manufacture of products with a large, continuous load [13]. It is only suitable for debugging the stress of die-casting machine.

The current research on tie-bar stress of the die-casting machine mainly focuses on simulation and theoretical analysis. Chang [14] established the evaluation indices based on the asymmetry of the mold/die clamping mechanism caused by mechanical errors. The presented research results would be helpful in tolerance analysis and mechanical error detection of nine-link-type double-toggle mold/die clamping mechanisms. Fu [15] constructed the multibody dynamic equation and optimized the different design parameters with the help of MSC.ADAMS software. The results after optimization revealed that clamping force was added to 3.25×10^7 N, and the course of clamping mold was more stable.

In 1986, Phani et al. [16] established the relationship between the propagation velocity of sound waves in materials and the stress, laying the foundation for acoustoelastic theory. After that, acoustoelastic theory was widely used in stress measurement [17,18]. Kim et al. [19] applied acoustoelastic theory to the measurement of bolt pretightening force. They used phase detection technology to measure sound wave propagation time. Experiments confirmed a good linear relationship between bolt stress and ultrasonic sound velocity. Ayadi et al. [20] proposed the use of acoustoelastic as a nondestructive method to monitor changes in the resistance of muscle fibers, unaffected by connective tissue. Our group [21,22] proposed an *in situ* clamping force measurement method for injection molding machine. Experiments verified this method is suitable for molds of different thickness and different scale injection molding machines. However, relevant research has not been carried out on stress of tie-bar for die-casting machine, and a simple, effective stress measurement method is lacking.

Based on acoustoelastic theory, a method of real-time measurement of tie-bar stress using ultrasonic technology is proposed in this paper. The mathematical model is established between ultrasonic signal and stress. Indirect calibration and cross-correlation function method are used to calculate material coefficient K_1 and ultrasonic time difference Δt in the mathematical model, respectively. The magnetic-attached strain gauge is used to verify the accuracy of the ultrasonic method. In addition, verification experiments, single-factor experiments, and applicability experiments were carried out. This paper is the first attempt to measure tie-bar stress through ultrasonic technology in die-casting machine. Online monitoring and measurement of stress level in tie bars of high-pressure die casting machine by ultrasonic measurement is critical for Industry 4.0. Ultrasonic equipment has a stronger anti-interference ability to adapt to higher temperature and worse die-casting environment under Industry 4.0. Moreover, the ultrasonic method can invert the dynamic information of die casting, which helps integrate with the controller to guide the efficient, safe production. Therefore, the measurement method has the advantages of high precision, high repeatability, easy installation, noninterference, wide application, real-time, nondestruction, and safety.

2 Theoretical analysis

2.1 Establishment of ultrasonic-stress mathematical model

Understanding the mechanical phenomena involved in die casting is very important to obtain high-quality castings. This paper first analyzed the stress variation of tie-bar in die casting. Then, the relationship between stress and strain was investigated. Combined with acoustoelastic theory, the mathematical relationship between ultrasonic signal and stress was established.

2.1.1 Analysis of stress variation

In die casting, the linkage assembly pushes the movable platen forward under the action of the clamp cylinder. Then, the movable platen moves forward to close the mold. Figure 1(a) shows that after the mold is closed, clamping force is finally applied to the four tie-bars through the movable platen, the fixed platen, and the rear platen. The stress of the tie-bar jumps from 0 to σ. In mold clamping, the four tie-bars of the die-casting machine are in a stretched state, whereas in mold opening, as shown in Fig. 1(b), the movable platen retreats and the stress returns to zero [23]. At this time, the tie-bars are in a relaxed state. Therefore, in large-scale industrial production, the mold of the die-casting machine is opened and closed alternately, and the stress on the tie-bar is applied alternately.

2.1.2 Formula derivation

The stress of the tie-bar is related to its deformation and elastic modulus, as shown in Eq. (1):

$$\sigma = E\varepsilon, \tag{1}$$

where σ is the stress of the tie-bar, E is the elastic modulus, and ε is the strain.

The magnitude of stress is determined by deformation because elastic modulus E is only related to the material properties. The deformation of the tie-bar is extremely small during mold clamping, and direct measurement of the deformation causes a large error. This paper adopts the method of indirect measurement and first analyzes its mathematical expression, as shown in Eq. (2):

$$\varepsilon = \frac{s_1 - s_0}{s_0} = \frac{\Delta s}{s_0}, \tag{2}$$

where s_0 is the natural length of the tie-bar with no stress, s_1 is the length of the tie-bar with σ stress, and Δs is the stretch length , as shown in Fig. 2.

The length of the tie-bar can be characterized by ultrasonic signals, as shown in Eqs. (3) and (4):

$$s_0 = v_0 \times \frac{1}{2} t_0, \tag{3}$$

$$s_1 = v_\sigma \times \frac{1}{2} t_1, \tag{4}$$

where t_0 and v_0 are the ultrasonic propagation time and the velocity with no stress, respectively, and t_1 and v_σ are the ultrasonic propagation time and the velocity with σ stress, respectively. The above formula alone cannot

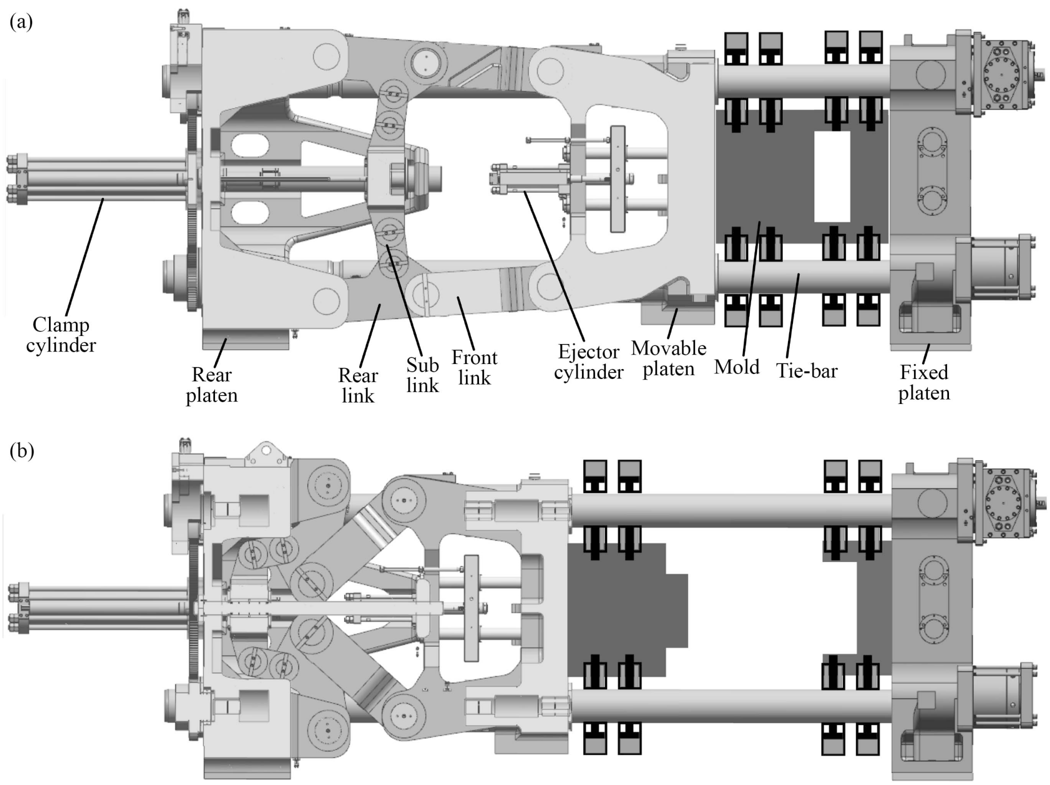

Fig. 1 Schematic diagram of tie-bars under different stress states: (a) mold clamping, (b) mold opening.

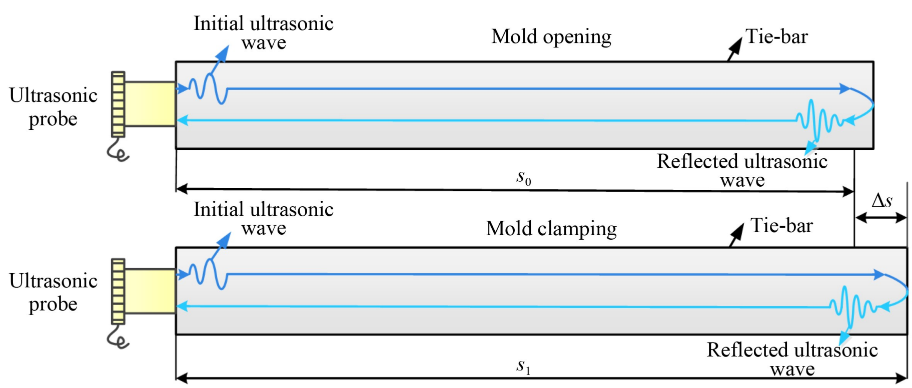

Fig. 2 Schematic diagram of deformation of tie-bar in die casting.

solve stress σ. Thus, it is combined with acoustoelastic theory for further derivation.

Acoustoelastic theory refers to the change of the sound velocity of an elastic material under the action of the initial static stress field. As reflected in this article, the propagation speed of the ultrasonic wave changes with the change of the stress of the tie-bar. The propagation speed of ultrasonic waves in it is also constantly changing because the tie-bar bears alternating stress in the cycle of mold closing and mold opening. The corresponding relationship between the ultrasonic propagation velocity and the stress of the tie-bar under the acoustoelastic effect is as follows [24]:

$$\rho_0 \times v_\sigma^2 = \lambda + 2\mu + \frac{\sigma}{3\lambda + 2\mu}\left[2l + \lambda + \frac{\lambda + \mu}{\mu}(4m + 4\lambda + 10\mu)\right], \tag{5}$$

where ρ_0 is the density of the tie-bar, λ and μ are the second-order elastic coefficients, and l and m are the third-order elasticity coefficients. When $\sigma = 0$, Eq. (5) is expressed as follows:

$$\rho_0 \times v_0^2 = \lambda + 2\mu. \tag{6}$$

Equation (6) is subtracted from Eq. (5) to obtain the following expression:

$$\begin{aligned}&\rho_0 \times (v_\sigma + v_0)(v_0 - v_\sigma)\\ &= \frac{\sigma}{3\lambda + 2\mu}\left[2l + \lambda + \frac{\lambda + \mu}{\mu}(4m + 4\lambda + 10\mu)\right],\end{aligned} \tag{7}$$

owing to $v_\sigma + v_0 \approx 2v_0$ and $\rho_0 = (\lambda + 2\mu)/v_0^2$, Eq. (7) is simplified to the following expression:

$$1 - \frac{v_\sigma}{v_0} = K\sigma, \tag{8}$$

where $K = \dfrac{2\mu + \lambda\mu + (\lambda + \mu)(4m + 4\lambda + 10\mu)}{2\mu(3\lambda + 2\mu)(\lambda + 2\mu)}$ is the acoustoelastic coefficient.

Then Eqs. (3), (4), and (8) are combined, and Eq. (9) is obtained as follows:

$$\frac{t_\sigma}{t_0} - 1 = \frac{\sigma}{E} \cdot \frac{1 + KE}{1 - K\sigma}, \tag{9}$$

when $K\sigma \ll 1$, the equation can be reduced to the following:

$$\sigma = K_1 \times \Delta t, \tag{10}$$

where $\Delta t = t_\sigma - t_0$ is the time difference between the ultrasonic wave when stress is σ and the time when stress is 0. This formula integrates elastic modulus E and acoustoelastic coefficient K into one parameter $K_1 = \dfrac{1}{(1/E + K)t_0}$, which is called the material coefficient of the tie-bar. By measuring ultrasonic propagation time under a known pulling force, combined with Eq. (10), parameter K_1 can be obtained.

In conclusion, the relationship between the stress and the strain of the tie bar, as shown in Eq. (1), is changed to the relationship between stress and ultrasonic propagation time, as shown in Eq. (10), based on acoustoelastic theory. After that, ultrasonic propagation time is calculated by the cross-correlation method, and the stress of the tie bar under different clamping states can be obtained according to Eq. (10).

2.2 Calculation of parameters in mathematical model

2.2.1 Calibration of parameter K_1

In Section 2.1, a unified character K_1 was used to indicate the material's elastic modulus E and acoustoelastic coefficient K. If K_1 is calculated directly, the parameters included that are difficult to determine due to the structure and processing technology of the tie-bar need to be measured accurately. For tie-bars on different die-casting machines and even on the same machine, the material coefficients are different, which brings great difficulties in direct calculation. In this paper, indirect calculation is used to calibrate the material coefficient K_1 of the tie-bar. After setting a series pulling force on the die-casting machine, the stress on the tie-bar and the Δt of the ultrasonic echoes can be measured by the strain gauge and the ultrasonic equipment. Linear regression can be performed with the measurement results with the intercept set as zero, and the slope of this line is material coefficient K_1.

Although the material coefficient K_1 of the tie-bar of the die-casting machine is obtained indirectly under certain experimental conditions, material coefficient K_1 is a physical quantity that characterizes the material itself and does not change with the experimental conditions. If the tie-bar of the die-casting machine remains unchanged, regardless of changing the process parameters, the molds, or the ultrasonic measurement systems, material coefficient K_1 remains the same. Therefore, all the experimental results below are based on the material coefficient K_1 measured in this section.

2.2.2 Calculations of parameter Δt

In this paper, the cross-correlation method is used to calculate ultrasonic propagation time difference Δt. The essence of this method is the overall overlap between two ultrasonic echo curves at different times [25–28]. It uses all the data between the two curves and has the advantages of higher accuracy and better repeatability.

2.2.3 Analysis of measurement accuracy

Measurement error represents the degree of agreement between the ultrasonic measurement results and the strain gauge results, which is represented by difference square $\overline{\delta}$ here, as defined in Eq. (11):

$$\bar{\delta} = \frac{1}{n} \times \sum_{i=1}^{n} (\sigma_i - \sigma_j)^2, \tag{11}$$

where σ_i is the stress measured by the strain gauge, σ_j is the stress measured by the ultrasonic method, and n is the number of experiments, $n = 5$.

3 Experiment

3.1 Experimental equipment

Figure 3 shows that the experiment equipment includes two parts: (1) ultrasonic measuring device and (2) verification device.

(1) The ultrasonic measuring device is composed of a signal receiving and transmitting instrument, a digital oscilloscope, and ultrasonic probes of various frequencies. The signal receiving and transmitting instrument (CTS-8077PR, Shantou Institute of Ultrasonic Instruments Co., Ltd., China) can generate different kinds of excitation signals. Its signal-to-noise ratio ranges from −50 to 60 dB, and it can filter the reflected ultrasonic signal. The digital oscilloscope (InfiniiVision DSO-X-2002A, Agilent Technologies Co., Ltd., USA) can visually display the ultrasonic signal curves and achieve complete data acquisition. The probe (Shantou Institute of Ultrasonic Instruments Co., Ltd., China) converts electrical signals and ultrasonic signals into each other. The selected probe is magnetic, which can be in close contact with the bottom of the tie-bar through magnetic force. The magnetic force is sufficient to ensure that the mechanical vibration generated in die casting does not affect ultrasonic measurement. Coupling agent is also applied between the probe and the tie-bar to prevent attenuation of ultrasonic signal caused by air.

(2) A magnetic-attached strain gauge (Monitor DU-1D, GEFRAN Sensors Co., Ltd., Italy) is selected as verification device and is referred to as strain gauge hereinafter. The strain gauge is directly fixed on the flat part of the tie-bar, close to the side of the stationary platen, to avoid errors caused by installation. The accuracy of the ultrasonic method can be verified by comparing the results of the ultrasonic measurement with the results of the strain gauge.

Finally, to facilitate the processing of experimental data, the four tie-bars are marked from #1 to #4.

3.2 Experimental scheme

Figure 4 shows that the experiment consists of three components: (1) verification experiments, (2) single-factor experiments, and (3) applicability experiments.

3.2.1 Verification experiments

The first part aimed to verify the accuracy of the ultrasonic measurement method. The magnetically attached ultrasonic probe (5P20) was installed on #3 tie-bar (The tie-bar was selected randomly, and other tie-bars were available). Then, the sampling frequency of the digital oscilloscope was set to 100 MHz, and the pulling force of the tie-bar was set to 100, 300, 500, 700, and 900 kN. The experiment in each stress state was repeated five times. Experimental data were collected by a digital oscilloscope and the strain gauge simultaneously.

3.2.2 Single-factor experiments

The second part aimed to find the influence of ultrasonic probe frequency, probe location, and different tonnages of die-casting machine on measurement accuracy. To prevent interference from other factors, the probe diameter and the sampling frequency were maintained at 20 mm and 100 MHz, respectively, and the experimental subjects all chose #3 tie-bar of Haitian HDC400 die-casting machine.

(1) In the experiment of the influence of ultrasonic probe frequency, ultrasonic probes with frequencies of 2.5, 5, and 10 MHz were selected. The largest difference from the verification experiment was that ultrasonic

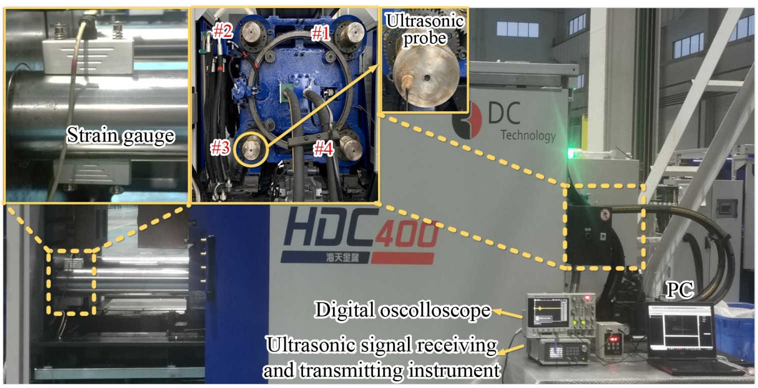

Fig. 3 Diagram of ultrasonic testing experimental system.

probes of different frequencies were chosen to carry out the experiments in a state of stress.

(2) In the experiment of the influence of ultrasonic probe location, ultrasonic probes with frequency of 5 MHz were chosen. In a state of stress, the experiments were performed by changing the location of the ultrasonic probe. Figure 5 shows that two probe locations were used for the experiments because of a positioning hole in the center of the tie-bar. One was near the positioning hole of the tie-bar, and the other was near the radius of the tie-bar.

(3) In the experiment of different tonnages of die-casting machines, Haitian HDC400 and HDC800 were selected as the experimental machines, and ultrasonic probes with a frequency of 5 MHz were used. When using HDC800, the tie-bar needed to be recalibrated, and the setting range of the pulling force of the tie-bar was wider, that is, from 200 to 1800 kN, with an interval of 400 kN.

The single-factor experiments can be regarded as parameter optimization, which can lay the foundation for subsequent applicability experiments.

3.2.3 Applicability experiments

The third part aimed to verify that the ultrasonic measurement method had wide application scenarios. This method was applied to monitor clamping health status and inspect dynamic changes in the pulling force of the tie-bar.

(1) Monitoring of clamping health status. The standard of die-casting machine mold clamping health status can be summarized as overall finiteness and uniformity of force distribution, that is, the pull force of a single tie-bar does not exceed the set threshold (generally 115% of maximum pulling force) and clamping force is evenly distributed (eccentric load rate is less than 5%). If the pulling force of the tie-bar exceeds the threshold, it may cause the most fragile tie-bar to break directly. The uneven distribution of the clamping force not only damages the mold but also causes the twisting and deformation of the tie-bar, and affects the accuracy of casting. In the experiment of monitoring of clamping health status, clamping force was approximately 2200 and 3200 kN. Then, in a state of stress, the ultrasonic signals of the four tie-bars were collected simultaneously.

(2) Inspection of dynamic changes in pulling force. The part aimed to reflect the change in the pulling force of the tie-bar in die casting. In the experiment, the working mode of the oscilloscope was set to continuous acquisition. Then, all signals of the dynamic opening and clamping of the tie-bar were collected.

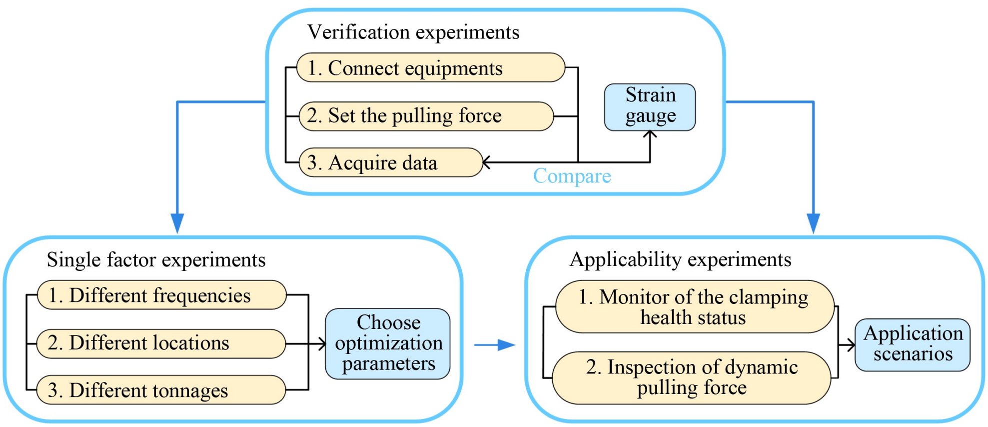

Fig. 4 Diagram of ultrasonic testing experiment.

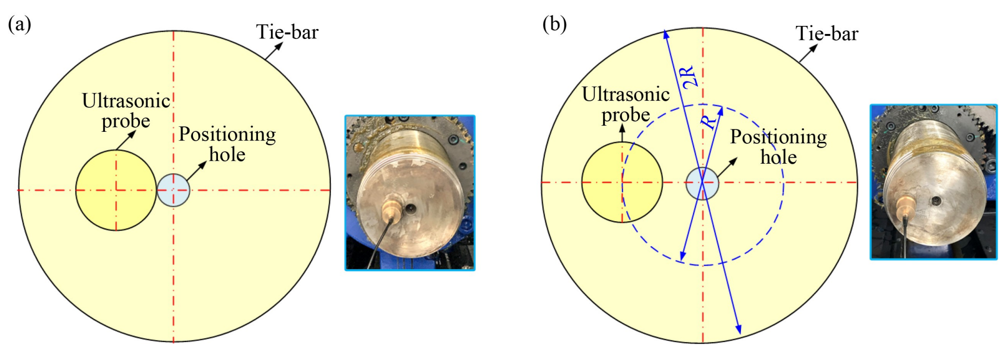

Fig. 5 Schematic diagram of probe location: (a) The probe is near the positioning hole, (b) the probe is near the radius of the tie-bar.

4 Results

4.1 Results of calibration of coefficient K_1

Figure 6 shows that the material coefficient of the four tie-bars of the die-casting machine (HDC400) was calibrated. The slopes of the four fitted curves were 0.05594, 0.05680, 0.05563, and 0.05698, and the R-square values were 0.99999, 0.99998, 0.99962, and 0.99992, which showed that the fitting method has a good imitative effect.

In the single-factor experiment, the influence of different tonnages of the die-casting machine on measurement accuracy was explored. The #3 tie-bar of the die-casting machine (HDC800) also needed to be calibrated in advance. Figure 7 shows that the slope and the R-square were 0.02012 and 0.99997, respectively. Moreover, the specific calibration coefficients of tie-bars of dissimilar materials were different.

4.2 Results of verification experiments

According to the calibration results in Section 4.1, combining with Δt calculated by the cross-correlation method and Eq. (10), the stress of #3 tie-bar was acquired. The different results of stress measurement of the two methods are shown in Fig. 8 and listed in Table A1. The difference square $\bar{\delta}$ values were 1.5678, 1.3876, 0.3181, 0.0234, and 0.0696 (MPa)^2 with the pulling force increasing from 100 to 900 kN. The maximum of the difference square $\bar{\delta}_{max}$ was only 1.5678 (MPa)^2. It proved that the ultrasonic method could measure stress with a high accuracy.

Moreover, standard deviation r was used to assess the stability of the measurement result, as shown in Eq. (12):

$$r = \frac{1}{n} \times \sqrt{\sum_{i=1}^{n} (\sigma_i - \bar{\sigma})^2}, \tag{12}$$

where $\bar{\sigma}$ is the average of n ($n = 5$) measurement results. The standard deviation of the measurement of the strain gauge is r_s, and the standard deviation of the measurement of the ultrasonic method is r_u. Table A1 shows that the standard deviation r_s values of the measurement of the strain gauge were 0.0486, 0.0118, 0.0862, 0.0636, and 0.0411 MPa, whereas the standard deviation r_u values of the measurement of the ultrasonic method were always 0 with the pulling force increasing from 100 to 900 kN. It proved that the ultrasonic method has a good measurement stability.

4.3 Results of single-factor experiments

4.3.1 Influences of ultrasonic probe frequency

The measurement results of two methods with different ultrasonic probe frequencies are shown in Fig. 9 and

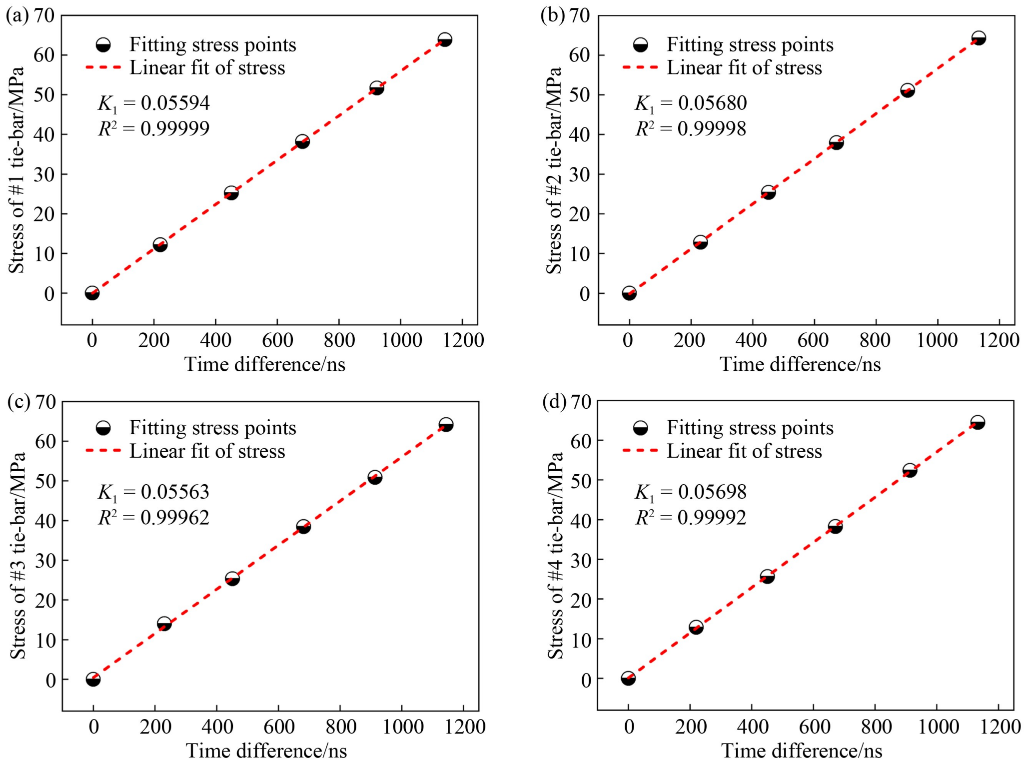

Fig. 6 Calibration results of material coefficient of four tie-bars (HDC400). (a) #1, (b) #2, (c) #3, and (d) #4.

listed in Table A2. Figure 9 shows that the frequency of the ultrasonic probe influences measurement accuracy. Table A2 shows that the mean of difference squares $\bar{\delta}_{ave}$ at 2.5 and 5 MHz were 2.3234 and 0.6733 (MPa)^2, respectively. The probe with center frequency of 5 MHz showed a higher accuracy.

This phenomenon can be explained by the beam characteristics in the propagation of ultrasonic wave. When the ultrasonic wave propagates in a slender tie-bar, it does not move in an absolute straight line. As propagation distance increases, the sound beam gradually diverges. The magnitude of this divergence can be characterized by the half divergence angle [29,30]. The specific formula of the half divergence angle is as follows:

$$\theta_0 \approx 70\frac{w}{D}, \tag{13}$$

where θ_0 is the half divergence angle of the ultrasound, w is the wavelength, and D is the diameter of the probe crystal element. A positive correlation exists between half divergence angle and wavelength. The relationship between ultrasonic frequency and wavelength is given by Eq. (14) [31]:

$$w = \frac{v}{f}, \tag{14}$$

where v is the ultrasonic wave speed (which changes slightly in this article), and f is the ultrasonic probe frequency. Clearly, the wavelength becomes shorter as the frequency of the ultrasonic wave increases, and the half emission angle becomes smaller. Therefore, measurement effect improves, and accuracy increases. However, if probe frequency is further increased (such as 10 MHz), the signal is attenuated excessively during propagation, and experimental error may be greater. In summary, increasing ultrasonic frequency in a certain range is beneficial to improving measurement accuracy.

4.3.2 Influences of ultrasonic probe location

The measurement results of two methods with different ultrasonic probe locations are shown in Fig. 10 and listed in Table A3. The figure shows that the frequency of

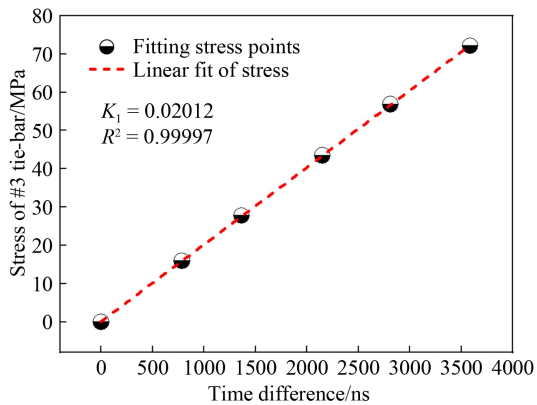

Fig. 7 Calibration results of material coefficient of #3 tie-bar (HDC800).

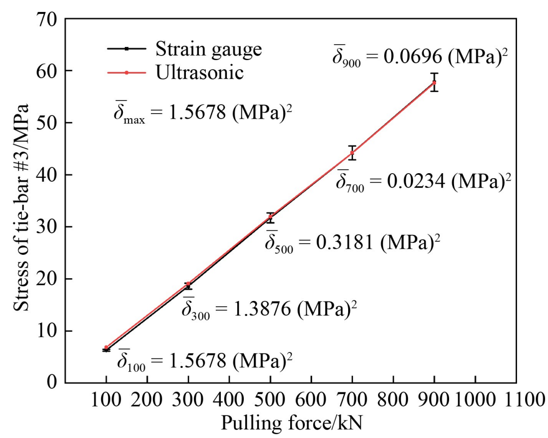

Fig. 8 Measurement results of ultrasonic and strain gauge of #3 tie-bar.

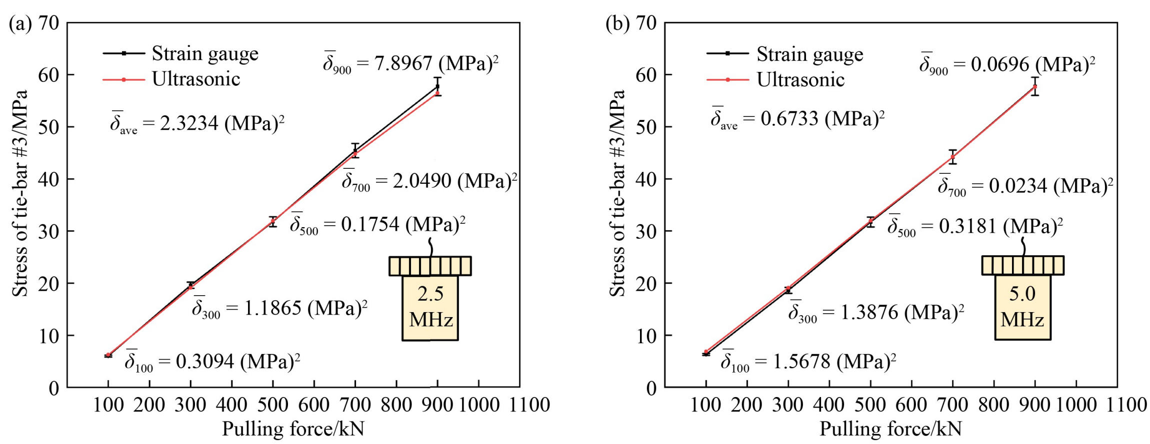

Fig. 9 Measurement results of ultrasonic and strain gauge of #3 tie-bar with different ultrasonic probe frequencies: (a) 2.5 MHz, (b) 5.0 MHz.

ultrasonic location has a minimal influence on measurement accuracy. Table A3 shows that the mean of difference squares $\bar{\delta}_{\text{ave}}$ near the positioning hole and near the radius were 0.6733 and 0.0105 (MPa)^2, respectively. The probe near the radius exhibited a slightly higher accuracy.

This result may be because the positioning hole at the center of the tie-bar changed the stress distribution around it. The location of the ultrasonic probe should be as far as possible from the center hole and the edge. However, given special installation requirements, the probe close can also be placed near the positioning hole.

4.3.3 Influences of tonnage of die-casting machine

The measurement results of two methods with different die-casting machines are shown in Fig. 11 and listed in Table A4. Figure 11 shows that the die-casting machine is not sensitive to measurement accuracy. The table shows that the mean of difference square $\bar{\delta}_{\text{ave}}$ values of HDC400 and HDC 800 were 0.0105 and 0.0332 (MPa)^2, respectively. The measurement results agree with the results of the magnetic-attached strain gauge, which meet the accuracy requirements of industrial testing. In summary, the ultrasonic method can be applied to different tonnages of die-casting machine and has good applicability and popularization.

4.4 Results of applicability experiments

4.4.1 Monitoring of clamping health status

The measurement results of two methods are shown in Fig. 12. When clamping force was 2200 kN, the pulling forces of tie-bars #1, #2, #3, and #4 were 568.89, 545.77, 566.49, and 544.44 kN, respectively. When clamping force was 3200 kN, the pulling force of tie-bars #1, #2, #3, and #4 were 803.83, 779.45, 816.66, and 792.99 kN, respectively. Then, the clamping health status of the die-casting machine was judged as follows.

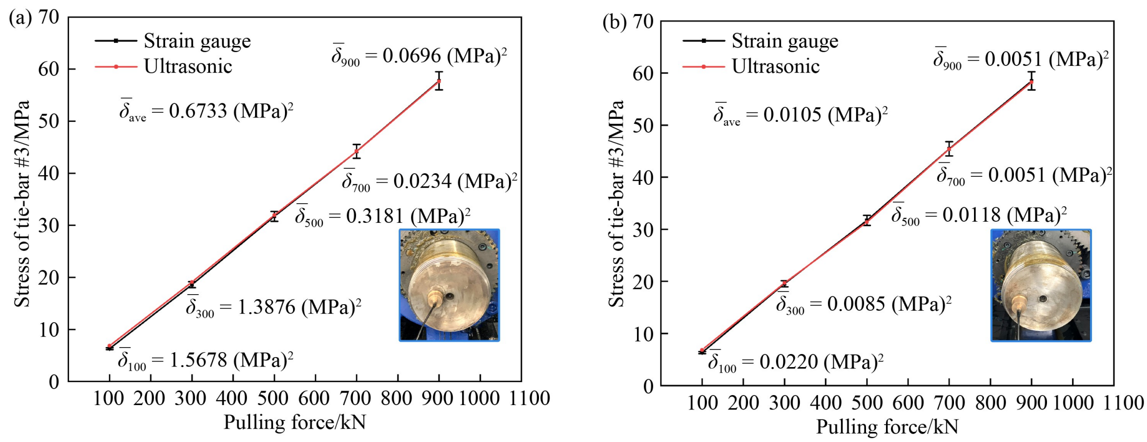

Fig. 10 Measurement results of ultrasonic and strain gauge of #3 tie-bar of different ultrasonic probe locations: (a) near positioning hole, (b) near radius.

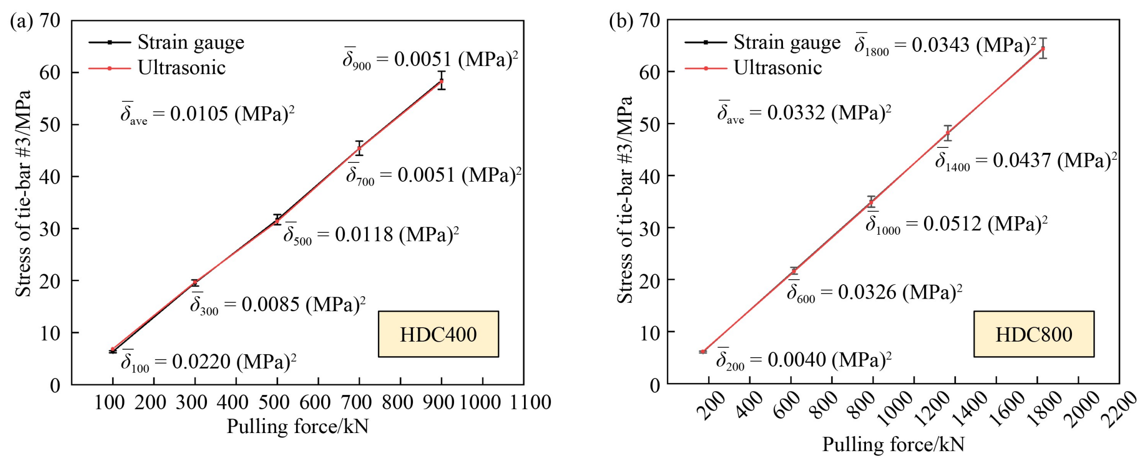

Fig. 11 Measurement results of ultrasonic and strain gauge of #3 tie-bar with different tonnages of die-casting machine: (a) HDC400, (b) HDC800.

1) Judgment of overall finiteness: 816.66 kN < 1000 kN × 115% = 1150 kN.

2) Judgment of uniformity of force distribution: (568.89 – 544.44)/550 ≈ 4.45% (clamping force was 2200 kN), (816.66 – 779.45)/800 ≈ 4.65% (clamping force was 3200 kN), which are all less than 5%.

In summary, this section determined that the pulling force of the Haitian HDC400 die-casting machine was limited and uniform. Thus, the clamping health status of the die-casting machine is qualified and does not require maintenance.

4.4.2 Inspection of dynamic pulling force

Figure 13 shows that the dynamic change of the pulling force of the tie-bar in die casting was measured by using the ultrasonic method. Dynamic change was divided into three stages: rising period, volatility period, and steady period. In 0–0.55 s, pulling force increased gradually during mold clamping. In 0.55–1.60 s, pulling force slightly fluctuated between 995 and 1005 kN, which may be related to the uneven distribution of friction in the high-pressure clamping stage and was controllable. After 1.60 s, mold clamping was completed, and pulling force was in a stable state. In summary, this method can invert dynamically the change of the pulling force of the tie-bar in die casting, which is helpful to guide subsequent production of die-casting products.

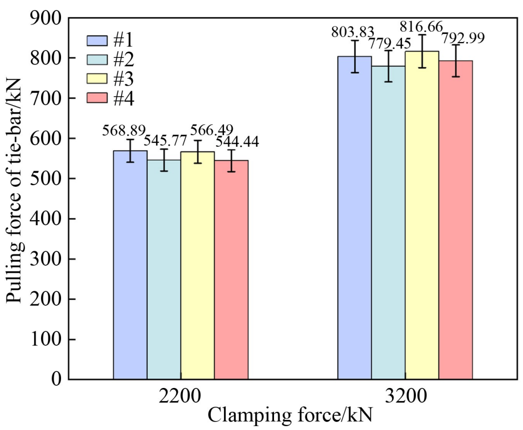

Fig. 12 Measurement results of pulling force of tie-bar on HDC400 Haitian die-casting machine.

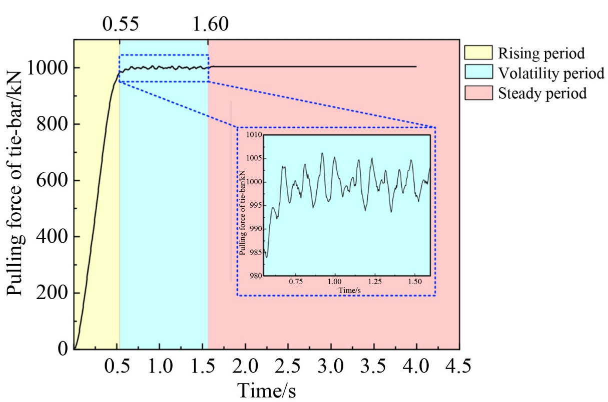

Fig. 13 Change of pulling force of tie-bar in die casting.

5 Discussion

Compared with the existing stress test methods, the ultrasonic method is more suitable for measuring the stress of the tie-bar. Discussion was carried out according to the applicability of the ultrasonic method in high-pressure die casting, condition of validation, and limitation in a real case. The relevant advantages are summarized as follows.

(1) Validation: The ultrasonic measurement method has high precision and high reliability. Compared with the strain gauge measurement results, the results of ultrasonic measurement show that the maximum of the difference square $\bar{\delta}_{max}$ is only 1.5678 $(MPa)^2$, which meets the precision requirements of industrial production. Moreover, the mean of standard deviation r_s of the measurement of the strain gauge is 0.05062 MPa, whereas the standard deviation r_u of the measurement of the ultrasonic method is always 0. The results prove that the ultrasonic method has good measurement reliability.

(2) Applicability: First, ultrasonic equipment is easy to install and characterized by noninterference. The ultrasonic sensor is magnetically attracted to the bottom of the tie-bar, which does not hinder the collection of die castings. Second, this method can continuously collect data for a period in real time, unlike strain gauges that can only collect data at a certain moment. This method can monitor the dynamic information of die casting online. Lastly, the intensity of the ultrasonic signal is almost unaffected by the length of the tie bar. This method is suitable for die casting machines of different tonnages. In summary, the ultrasonic device is easy to install and suitable for almost all die casting machines.

(3) Limitation: The dynamic collection of die-casting production information puts forward higher requirements on the ultrasonic acquisition card. In addition, operation environments such as high temperature and strong electricity may reduce the signal-to-noise ratio of the signal and deteriorate measurement accuracy. In these cases, more advanced signal processing methods should be introduced to increase robustness.

6 Conclusions

In this paper, the mathematical model of ultrasonic signal and stress was established, and an ultrasonic method to measure the stress of tie-bar in die casting was proposed. Then, a series of verification experiments, single-factor experiments, and applicability experiments, were implemented. Based on the results, the following conclusions can be drawn:

(1) The ultrasonic measurement method has a high accuracy, with a difference square of less than 1.60 $(\mathrm{MPa})^2$.

(2) The increase in ultrasonic frequency within a certain range is beneficial to improving measurement accuracy. As ultrasonic frequency varies from 2.5 to 5 MHz, the mean of difference square varies from 2.3234 to 0.6733 $(\mathrm{MPa})^2$, and measurement accuracy is insensitive to the probe location and the tonnage of die-casting machine.

(3) The proposed method can be applied in various scenarios such as monitoring of clamping state and inspection of dynamic pulling force of tie-bar.

Finally, the ultrasonic method for measuring the stress of the tie-bar has the advantages of high precision, high repeatability, easy installation, noninterference, and wide application. The ultrasonic measurement method can provide reference for online adjustment of tie-bar stress. It can effectively improve production efficiency of die-casting products while protecting the mold and the machine itself.

Nomenclature

D	Ultrasonic probe diameter
E	Elastic modulus
f	Ultrasonic probe frequency
K	Acoustoelastic coefficient
K_1	Material coefficient
l, m	The third-order elasticity coefficients
n	Number of experiments
Δt	Ultrasonic time difference
r	Standard deviation
r_s	Standard deviation of strain gauge
r_u	Standard deviation of ultrasonic
s_0	Natural length of the tie-bar with no stress
s_1	Length of the tie-bar with σ stress
t_0	Ultrasonic propagation time with no stress
t_1	Ultrasonic propagation time with σ stress
v	Ultrasonic wave speed
v_0	Velocity with no stress
v_σ	Velocity with σ stress
w	Ultrasonic wavelength
σ	Stress of the tie-bar
σ_i	Stress measured by the strain gauge
σ_j	Stress measured by the ultrasonic method
ε	Strain
ρ_0	Density of the tie-bar
λ, μ	The second-order elastic coefficients
θ_0	Half divergence angle of the ultrasound
$\bar{\delta}$	Difference square
$\bar{\delta}_{ave}$	Mean of the difference squares
$\bar{\delta}_{max}$	Maximum of the difference square

Appendix

Table A1 Ultrasonic measurement results of verification experiments

Pulling force/kN	σ_i/MPa	σ_j/MPa	$\bar{\delta}/(\mathrm{MPa})^2$	$\bar{\delta}_{max}/(\mathrm{MPa})^2$	r_s/MPa	r_u/MPa
100	6.23628	6.8461				
	6.30124	6.8461				
	6.30124	6.8461	1.5678		0.0486	0
	6.23628	6.8461				
	6.36620	6.8461				
300	18.3840	19.1067				
	18.6439	19.1067				
	18.7088	19.1067	1.3876		0.0118	0
	18.6439	19.1067				
	18.5789	19.1067				
500	31.5711	31.9511				
	31.8310	31.9511				
	31.7011	31.9511	0.3181	1.5678	0.0862	0
	31.7660	31.9511				
	31.7011	31.9511				
700	44.1736	44.2117				
	44.1736	44.2117				
	44.1087	44.2117	0.0234		0.0636	0
	44.1736	44.2117				
	44.3035	44.2117				
900	57.7505	57.6399				
	57.7505	57.6399				
	57.8155	57.6399	0.0696		0.0411	0
	57.7505	57.6399				
	57.6855	57.6399				

Table A2 Measurement results of ultrasonic and strain gauge of #3 tie-bar with different ultrasonic probe frequencies

Probe frequency/MHz	Pulling force/kN	σ_i/MPa	Δt/ns	σ_j/MPa	$\bar{\delta}/(\mathrm{MPa})^2$	$\bar{\delta}_{ave}/(\mathrm{MPa})^2$
2.5	100	6.04139	104.948	6.2621		
		5.97643	104.948	6.2621		
		6.04139	104.948	6.2621	0.3094	
		6.04139	104.948	6.2621		
		5.97643	104.948	6.2621		2.3234
	300	19.5533	335.832	19.1062		
		19.6183	335.832	19.1062		
		19.5533	335.832	19.1062	1.1865	
		19.6183	335.832	19.1062		
		19.6183	335.832	19.1062		

Table A2 (Continued)

Probe frequency/MHz	Pulling force/kN	σ_i/MPa	Δt/ns	σ_j/MPa	$\bar{\delta}$/(MPa)^2	$\bar{\delta}_{ave}$/(MPa)^2
2.5	500	31.7011	566.717	31.9503		
		31.7660	566.717	31.9503		
		31.7011	566.717	31.9503	0.1754	
		31.8959	566.717	31.9503		
		31.8310	566.717	31.9503		
	700	45.4728	797.601	44.7945		
		45.4079	797.601	44.7945		
		45.4079	797.601	44.7945	2.0490	2.3234
		45.4728	797.601	44.7945		
		45.4079	797.601	44.7945		
	900	57.5556	1007.496	56.4709		
		57.8155	1007.496	56.4709		
		57.7505	1007.496	56.4709	7.8967	
		57.7505	1007.496	56.4709		
		57.7505	1007.496	56.4709		
5	100	6.23628	115.445	6.8461		
		6.30124	115.445	6.8461		
		6.30124	115.445	6.8461	1.5678	
		6.23628	115.445	6.8461		
		6.36620	115.445	6.8461		
	300	18.3840	335.840	19.1067		
		18.6439	335.840	19.1067		
		18.7088	335.840	19.1067	1.3876	
		18.6439	335.840	19.1067		
		18.5789	335.840	19.1067		
	500	31.5711	566.730	31.9511		
		31.8310	566.730	31.9511		
		31.7011	566.730	31.9511	0.3181	0.6733
		31.7660	566.730	31.9511		
		31.7011	566.730	31.9511		
	700	44.1736	787.125	44.2117		
		44.1736	787.125	44.2117		
		44.1087	787.125	44.2117	0.0234	
		44.1736	787.125	44.2117		
		44.3035	787.125	44.2117		
	900	57.7505	1028.510	57.6399		
		57.7505	1028.510	57.6399		
		57.8155	1028.510	57.6399	0.0696	
		57.7505	1028.510	57.6399		
		57.6855	1028.510	57.6399		

Table A3 Measurement results of ultrasonic and strain gauge of #3 tie-bar of different ultrasonic probe locations

Probe location	Pulling force/kN	σ_i/MPa	Δt/ns	σ_j/MPa	$\bar{\delta}$/(MPa)^2	$\bar{\delta}_{ave}$/(MPa)^2
Near positioning hole	100	6.23628	115.445	6.8461		
		6.30124	115.445	6.8461		
		6.30124	115.445	6.8461	1.5678	
		6.23628	115.445	6.8461		
		6.36620	115.445	6.8461		
	300	18.3840	335.840	19.1067		
		18.6439	335.840	19.1067		
		18.7088	335.840	19.1067	1.3876	
		18.6439	335.840	19.1067		
		18.5789	335.840	19.1067		
	500	31.5711	566.730	31.9511		
		31.8310	566.730	31.9511		
		31.7011	566.730	31.9511	0.3181	0.6733
		31.7660	566.730	31.9511		
		31.7011	566.730	31.9511		
	700	44.1736	787.125	44.2117		
		44.1736	787.125	44.2117		
		44.1087	787.125	44.2117	0.0234	
		44.1736	787.125	44.2117		
		44.3035	787.125	44.2117		
	900	57.7505	1028.510	57.6399		
		57.7505	1028.510	57.6399		
		57.8155	1028.510	57.6399	0.0696	
		57.7505	1028.510	57.6399		
		57.6855	1028.510	57.6399		
Near radius	100	6.3662	115.445	6.3272		
		6.4312	115.445	6.3272		
		6.3012	115.445	6.3272	0.0220	
		6.3012	115.445	6.3272		
		6.2363	115.445	6.3272		
	300	19.5533	346.335	19.5533		
		19.6183	346.335	19.5533		
		19.5533	346.335	19.5533	0.0085	
		19.5533	346.335	19.5533		
		19.4883	346.335	19.5533		
	500	31.7011	556.235	31.7141		
		31.7660	556.235	31.7141		
		31.7660	556.235	31.7141	0.0118	0.0105
		31.7011	556.235	31.7141		
		31.6361	556.235	31.7141		
	700	45.4728	808.115	45.4469		
		45.4079	808.115	45.4469		
		45.4079	808.115	45.4469	0.0051	
		45.4728	808.115	45.4469		
		45.4728	808.115	45.4469		
	900	58.4651	1039.005	58.4911		
		58.5300	1039.005	58.4911		
		58.4651	1039.005	58.4911	0.0051	
		58.5300	1039.005	58.4911		
		58.4651	1039.005	58.4911		

Table A4 Measurement results of ultrasonic and strain gauge of #3 tie-bar with different tonnages of die-casting machine

Mechanical tonnage/t	Pulling force/kN	σ_i/MPa	Δt/ns	σ_j/MPa	$\bar{\delta}$/(MPa)^2	$\bar{\delta}_{ave}$/(MPa)^2
400	100	6.3662	115.445	6.3272		
		6.4312	115.445	6.3272		
		6.3012	115.445	6.3272	0.0220	
		6.3012	115.445	6.3272		
		6.2363	115.445	6.3272		
	300	19.5533	346.335	19.5533		
		19.6183	346.335	19.5533		
		19.5533	346.335	19.5533	0.0085	
		19.5533	346.335	19.5533		
		19.4883	346.335	19.5533		
	500	31.7011	556.235	31.7141		
		31.7660	556.235	31.7141		
		31.7660	556.235	31.7141	0.0118	0.0105
		31.7011	556.235	31.7141		
		31.6361	556.235	31.7141		
	700	45.4728	808.115	45.4469		
		45.4079	808.115	45.4469		
		45.4079	808.115	45.4469	0.0051	
		45.4728	808.115	45.4469		
		45.4728	808.115	45.4469		
	900	58.4651	1039.005	58.4911		
		58.5300	1039.005	58.4911		
		58.4651	1039.005	58.4911	0.0051	
		58.5300	1039.005	58.4911		
		58.4651	1039.005	58.4911		
800	200	6.1017	298.8505	6.0664		
		6.1369	298.8505	6.0664		
		6.0311	298.8505	6.0664	0.0034	
		5.9606	298.8505	6.0664		
		6.1017	298.8505	6.0664		
	600	21.4793	1065.4670	21.7050		
		21.7262	1065.4670	21.7050		
		21.8320	1065.4670	21.7050	0.0326	
		21.7262	1065.4670	21.7050		
		21.7615	1065.4670	21.7050		
	1000	34.6702	1721.6388	34.9453		
		35.0934	1721.6388	34.9453		
		35.0229	1721.6388	34.9453	0.0512	0.0332
		34.9524	1721.6388	34.9453		
		34.9876	1721.6388	34.9453		
	1400	48.0022	2390.8040	48.1362		
		47.9317	2390.8040	48.1362		
		48.0375	2390.8040	48.1362	0.0434	
		48.3802	2390.8040	48.1362		
		48.3196	2390.8040	48.1362		
	1800	64.4026	3196.4010	64.4802		
		64.6143	3196.4010	64.4802		
		64.4379	3196.4010	64.4802	0.0343	
		64.5790	3196.4010	64.4802		
		64.3674	3196.4010	64.4802		

Acknowledgements The authors acknowledge the financial support of the Key Project of Science and Technology Innovation 2025 of Ningbo City, China (Grant No. 2020Z018), the “Pioneer” and “Leading Goose” R&D Program of Zhejiang Province, China (Grant No. 2022C01069), the National Natural Science Foundation of China (Grant No. 51875519), and the Project of Innovation Enterprises Union of Ningbo City, China (Grant No. 2021H002).

References

1. Shahane S, Aluru N, Ferreira P, Kapoor S G, Vanka S P. Optimization of solidification in die casting using numerical simulations and machine learning. Journal of Manufacturing Processes, 2020, 51: 130–141
2. Liu W P, Peng T, Tang R Z, Umeda Y, Hu L K. An internet of things-enabled model-based approach to improving the energy efficiency of aluminum die casting processes. Energy, 2020, 202: 117716
3. Greß T, Mittler T, Chen H, Stahl J, Schmid S, Khalifa N B, Volk W. Production of aluminum AA7075/6060 compounds by die casting and hot extrusion. Journal of Materials Processing Technology, 2020, 280: 116594
4. Lee J, Lee Y C, Kim J T. Migration from the traditional to the smart factory in the die-casting industry: novel process data acquisition and fault detection based on artificial neural network. Journal of Materials Processing Technology, 2021, 290: 116972
5. Weiler J P. A review of magnesium die-castings for closure applications. Journal of Magnesium and Alloys, 2019, 7(2): 297–304
6. Yoo M, Song J, Oh J, Kang S, Kim K, Yang S, Moon M. Development of a bus armrest fabrication process with a high-vacuum, high-pressure die-casting process using the AM60 alloy. Robotics and Computer-Integrated Manufacturing, 2019, 55: 154–159
7. Cornacchia G, Dioni D, Faccoli M, Gislon C, Solazzi L, Panvini A, Cecchel S. Experimental and numerical study of an automotive component produced with innovative ceramic core in high pressure die casting (HPDC). Metals, 2019, 9(2): 217
8. Jeong S I, Jin C K, Seo H Y, Kim J D, Kang C G. Mold structure design and casting simulation of the high-pressure die casting for aluminum automotive clutch housing manufacturing. The International Journal of Advanced Manufacturing Technology, 2016, 84: 1561–1572
9. Pisarek B P, Kołakowski D, Pacyniak T. Simulation of stress distribution in a thick-walled bushing produced by die-casting. Archives of Foundry Engineering, 2017, 17(4): 127–132
10. Cao H J, Chen E, Yi H, Li H C, Zhu L Q, Wen X H. Multi-level energy efficiency evaluation for die casting workshop based on fog-cloud computing. Energy, 2021, 226: 120397
11. Dong X X, Feng L Y, Wang S H, Nyberg E A, Ji S X. A new die-cast magnesium alloy for applications at higher elevated temperatures of 200–300 °C. Journal of Magnesium and Alloys, 2021, 9(1): 90–101
12. Rao B Q, Zhou H W, Ouyang H B, Wan Y J, Zhang Y H, Wu J Y. Study on the clamping force measurement and partial load

regulation technology of injection molding machine. CIRP Journal of Manufacturing Science and Technology, 2017, 19: 19–24

13. Chen J W, Schlaepher B. New measurement techniques of injection molding machine clamping force. Engineering Plastics Application, 2010, 38(2): 75−77 (in Chinese)
14. Chang W T, Lee W I, Hsu K L. Analysis and experimental verification of mechanical errors in nine-link type double-toggle mold/die clamping mechanisms. Applied Sciences (Basel, Switzerland), 2021, 11(2): 832
15. Fu K X, Zheng Z X, Zhang H W. Design of double-toggle clamping mechanism for die-casting machine based on the multi-body dynamics and finite element method. Applied Mechanics and Materials, 2013, 427–429: 179–186
16. Phani K K, Niyogi S K, Maitra A K, Roychaudhury M. Strength and elastic modulus of a porous brittle solid: an acousto-ultrasonic study. Journal of Materials Science, 1986, 21(12): 4335–4341
17. Prasath R, Danyluk S, Zagarola S. Non-contact stress measurement in PET preforms. Polymer-Plastics Technology and Materials, 2019, 58(16): 1802–1809
18. Bray D E, Tang W. Subsurface stress evaluation in steel plates and bars using the L_{CR} ultrasonic wave. Nuclear Engineering and Design, 2001, 207(2): 231–240
19. Kim J, Park J H, Jhang K Y. Decoupled longitudinal and lateral vehicle control based autonomous lane change system adaptable to driving surroundings. IEEE Access: Practical Innovations, Open Solutions, 2021, 9: 4315–4334
20. Ayadi A, Culioli J, Abouelkaram S. Sonoelasticity to monitor mechanical changes during rigor and ageing. Meat Science, 2007, 76(2): 321–326
21. Zhao P, Zhao Y, Zhang J F, Huang J Y, Xia N, Fu J Z. Ultrasonic measurement of clamping force for injection molding machine. Journal of Polymer Engineering, 2019, 39(4): 388–396
22. Zhao Y, Zhao P, Zhang J F, Huang J Y, Xia N, Fu J Z. On-line measurement of clamping force for injection molding machine using ultrasonic technology. Ultrasonics, 2019, 91: 170–179
23. Cecchel S, Cornacchia G, Panvini A. Cradle-to-gate impact assessment of a high-pressure die-casting safety-relevant automotive component. JOM, 2016, 68(9): 2443–2448
24. Tokuoka T, Iwashimizu Y. Acoustical birefringence of ultrasonic waves in deformed isotropic elastic materials. International Journal of Solids and Structures, 1968, 4(3): 383–389
25. Zeng L, Cao X W, Huang L P, Luo Z. The measurement of lamb wave phase velocity using analytic cross-correlation method. Mechanical Systems and Signal Processing, 2021, 151: 107387
26. Xiao W F, Yu L Y, Joseph R, Giurgiutiu V. Fatigue-crack detection and monitoring through the scattered-wave two-dimensional cross-correlation imaging method using piezoelectric transducers. Sensors (Basel), 2020, 20(11): 3035
27. Fan Z Q, Qiu Q, Su J, Zhang T H, Lin Y. Phase noise measurement of an optoelectronic oscillator based on the photonic-delay line cross-correlation method. Optics Letters, 2019, 44(8): 1992–1995
28. Li Y, Yu S S, Dai L, Luo T F, Li M. Acoustic emission signal source localization on plywood surface with cross-correlation method. Journal of Wood Science, 2018, 64(2): 78–84
29. Komura I, Nagai S, Kashiwaya H, Mori T, Arii M. Improved ultrasonic testing by phased array technique and its application. Nuclear Engineering and Design, 1985, 87: 185–191
30. Wang J G, Deng Z F, Yang B H, Ma S W, Fei M R, Liu L L, Yao Y, Chen T, Wu Y P. Simultaneous identification of parameter and time-delay based on subspace method and cross-correlation function. In: Proceedings of the 36th Chinese Control Conference (CCC). 2017, 2287–2292
31. Yamamoto N. New method of determining ultrasonic wavelength in liquid. Review of Scientific Instruments, 1954, 25(10): 949–950